Composites Part B 194 (2020) 108052

Contents lists available at ScienceDirect

Composites Part B

journal homepage: www.elsevier.com/locate/compositesb

Digital volume correlation technique for characterizing subsurface deformation behavior of a laminated composite

Sooyoung Lee, Eonyeon Jo [1], Wooseok Ji [*]

Department of Mechanical Engineering, Ulsan National Institute of Science and Technology (UNIST), Ulsan, South Korea

A B S T R A C T

In the present study, the digital volume correlation (DVC) technique is used to study the deformation behavior occurring inside a carbon fibre-reinforced epoxy composite. While a tensile test on a symmetric angle-ply laminated composite specimen is being performed, X-ray images are recorded using synchrotron radiation. The radiographs are processed to reconstruct 3D μCT images. The reconstruction process utilizes a filtered back-projection (FBP) algorithm combined with a phase retrieval method to enhance the contrast of the CT images. Phase contrast is crucial since the natural microstructural pattern is analogous to a speckle pattern for digital image correlation (DIC) analysis. A slight misalignment of the specimen, typically negligible at the macroscopic scale, is corrected in the CT images prior to the DVC analysis. The accuracy of the DVC results is improved by implementing a sub-voxel registration approach to achieve a resolution less than one pixel. The DVC results are compared with finite element analysis (FEA) results. Although the overall results agree well with the FEA results, few subvolumes are prone to fail to find their correct pairs within DVC volumes. Raw 2D tomograms are individually examined and compared to show that a high correlation coefficient value does not always guarantee a correct match. Detailed discussions about the misleading correlations are provided and thereby the validations and limitations of the DVC (and DIC) technique are addressed.

1. Introduction

Fiber-reinforced polymeric (FRP) composite materials have been widely used in commercial and military aerospace applications owing to their superior stiffness- and strength-to-weight ratios that monolithic materials cannot offer. The combination of two different materials yet introduces a unique micro-scale damage and failure mainly caused by the significant stiffness mismatch between the fiber and the polymeric matrix material. Furthermore, the evolution of the subsurface damage is a very complicated process due to the heterogeneous microstructural morphology of the composites. Comprehensive understanding of the complex subsurface damage behavior can be achieved by observing various failure processes occurring inside the composite materials and characterizing them with quantitative measurements of subsurface deformation. However, such a data requires a special technique for mapping full-field strain data into the whole volume of a specimen, which cannot be achieved by traditional strain measurement methods. Digital image correlation technique (DIC) is capable of computing full-field strain data of a deformable sample by tracking an artificial black-and-white speckle pattern between images sequentially taken while the specimen is being loaded. Although the DIC technique is now widely used to investigate the progressive damage and failure response of the composite materials in real time, the DIC results are limited on the specimen surface where the speckle pattern is applied [1].

X-ray micro-computed tomography (μCT) is one potential approach to observe the subsurface deformation behavior of a material through 3D volumetric images at a sub-micron resolution. Owing to the recent development of tomography techniques and resources, X-ray μCT-based *in situ* experimentation has been utilized to visualize the microstructural behavior of the composite materials. Spearing and his team performed extensive studies to *in situ* observe and visualize multiple failure modes occurring inside a symmetric cross-ply laminated composite with double notches using a synchrotron X-ray source [2–5]. Ueda. et al. performed compression tests on uni-directionally continuous fiber-reinforced composite coupons to observe the formation of kink bands [6]. The team of Ritchie observed damage mechanisms in ceramic matrix composites under tensile loading at elevated temperatures using synchrotron X-rays [7]. Li et al. performed *in situ* loading tests on three-dimensionally woven textile composites using synchrotron radiation and investigated out-of-plane failure mechanisms under tensile and shear loading conditions [8].

Nowadays, with the association of X-ray μCT acquisitions, the digital volume correlation (DVC) technique has been effectively used to quantitatively measure internal deformation behavior of various materials

* Corresponding author.
E-mail address: wsji@unist.ac.kr (W. Ji).
[1] Currently at LG Hausys R&D Center, Seoul, S. Korea.

https://doi.org/10.1016/j.compositesb.2020.108052
Received 23 October 2019; Received in revised form 22 March 2020; Accepted 6 April 2020
Available online 12 April 2020
1359-8368/

[9–12]. The DVC method can be considered as the extended version of the DIC approach to a three-dimensional (3D) domain, dealing with CT image data [13]. The DVC technique requires high-contrast 3D CT images with a wide variation of grayscale values for accurate measurements, similarly as the DIC technique is heavily dependent on a speckle pattern. The grayscale contrast on 3D CT images may be resulted from the natural microstructures of heterogeneous materials such as wood [11] and bone [13]. In case of isotropic homogeneous materials, some microparticles can be embedded during a specimen fabrication process in order to enhance the image contrast by means of a 3D volumetric speckle pattern [9,14]. Few researchers have implemented the DVC technique for composite materials reinforced with either particles or fibers. Mostafavi et al. has performed *ex situ* indentation tests on Al–SiC metal matrix composites and investigated the subsurface deformation underneath the indenter through DVC analysis [12]. Their team could obtain sufficient grayscale contrast owing to the density difference between the two constituents of the specimen. Brault et al. has embedded copper powder between interlayers of carbon-epoxy prepregs in order to overcome the similar densities between the carbon and epoxy materials and enhance the contrast in 3D CT images [15]. They performed *in situ* three-point bending tests with the particle-filled composite specimens. These two studies highlight the importance of strong grayscale contrast in 3D CT images for the successful implementation of the DVC approach, especially for materials composed of more than two materials with similar densities like fiber/epoxy composites. To the best of the authors' knowledge, the DVC technique has not been utilized for *in situ* tensile test data of "pure" carbon fibre-reinforced polymeric materials without an inclusion improving image contrast.

In the present study, the DVC technique is employed to measure the deformation behavior inside a carbon fibre-reinforced epoxy composite. While a tensile test on a symmetric angle-ply laminated composite specimen with the stacking sequence of $[+45/-45]_S$ is being performed, 3D μCT images are recorded at Beamline 6C in Pohang Acceleration Laboratory (PAL). Since the natural microstructural pattern is used for the DVC analysis, the potential contrast deficiency in 3D CT images of the carbon-epoxy specimen is overcome by optimal experimental settings with the synchrotron light source combined with the state-of-the-art image reconstruction technique. A special loading frame for *in situ* testing customized at the synchrotron facility [1] and an in-house DVC algorithm, developed by the authors' previous work [14], are utilized for the present study. The DVC algorithm is augmented with a pre-processing function to correct a slight initial misalignment of the specimen and remove rigid-body motions during the test. In addition, a sub-voxel registration scheme is appended to improve the measurement resolution. Detailed descriptions about the implementation of the DVC technique for the carbon/epoxy composite will be provided in the following sections.

The rest of this paper is organized as follows. Section 2 describes in great detail the *in situ* mechanical testing protocol using the synchrotron light source for the DVC analysis of the carbon-epoxy composite specimen. Section 3 presents the working principles of each pre- and post-processing approaches implemented into the present DVC technique. The results of the pre- and post-processes are discussed in Sections 4.1 and 4.2. In Section 4.3, DVC analysis results of the composite specimen are presented and compared with finite element analysis (FEA) results for the purpose of validation. Section 4.4 discusses validities and limitations of implementing the DVC approach for the composite material. The conclusions of the present study are summarized in Section 5.

2. Experimental procedure

2.1. Test specimens

The present study considers unidirectionally continuous fiber-reinforced laminated composites. Prepregs with a material system of UIN150/H15 (SK Chemicals, South Korea) were utilized to fabricate test specimens with the stacking sequences of $[+45_2/-45_2]_S$. Fig. 1 shows the configuration of the test specimens. The specimens were designed to have very long grip areas as shown in Fig. 1(a) in order to prevent slippage during tension tests. Round notches were introduced on both sides of the specimens to intensify stresses at the central region, so that the location of failure initiation was predictable. Detailed dimensions of the notches can be found in Fig. 1(b). A waterjet cutter was utilized to carve the specimens from a panel having the thickness of 1.13 mm. The cutter left no particular flaw to the specimen, especially in the notch tip surface as seen in the authors' previous work (see Fig. 2(b) of [1]).

2.2. Mechanical testing during X-ray imaging

X-ray images were recorded while the double-edge notched symmetric angle-ply laminate specimen was being loaded. As illustrated in Fig. 2(a), the X-ray beam penetrated through the sample installed in the loading device. A motorized positioning stage was utilized to precisely locate the sample with respect to the beam path. The loading device was specifically designed to be used in the beamline and its performance has been demonstrated in Ref. [1] for the *in situ* observation of a cross-ply laminate specimen subjected to tensile loading. Fig. 2(b) shows the actual testing setup on the beamline testbed.

Displacement-controlled loading was applied to the specimen and a specific displacement was maintained while X-ray images were being taken. X-ray scanning was carried out at 5 steps from 0 to 0.08 mm with the interval of 0.02 mm, in terms of the crosshead displacement. At each of the five loading steps, X-ray projection images (radiographs) were recorded at every 0.25° as the testing instrument was rotated stepwise through the total angular range of 180° with the exposure time of 2.5 s per projection. Compared to the conventional polychromatic X-ray CT, synchrotron CT provides monochromatic X-ray beam and beam-hardening effect is negligible [16]. Therefore, X-ray scanning over the 180-degree rotation is perfectly mirror-symmetric.

2.3. X-ray acquisition setup

The subsurface deformation behavior of the composite material was imaged at Beamline 6C in Pohang Accelerator Laboratory (PAL). The monochromatic parallel X-ray beam from the synchrotron light source was modulated at a photon energy of 24 keV. This energy level was high enough to penetrate the sample at least 10% in transmission, but low enough to enhance image contrast for good image quality [16]. In this section, the basic concept of X-ray physics [17] will be briefly introduced first in order to discuss an optimal photon energy setting for X-ray tomography. In general, X-ray radiography utilizes different radiation absorption capabilities of materials. As X-ray beams pass through a particular object, photons are absorbed, which reduces the beam energy. This phenomenon is known as the photoelectric effect in which the composing atoms of an object absorb photon energy and emit electrons. The energy absorbed by a particular object is mainly dependent on its density and attenuation coefficient, μ. The differences in the energy absorption rate are eventually correlated with a specific gray-scale value in a radiograph. The higher the density (also μ) of an object, the darker it will be imaged on the radiograph. The grayscale contrast in the

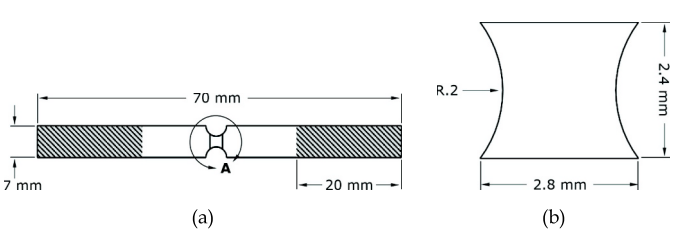

Fig. 1. (a) Dimensions of the double-edge-notched specimen (b) Detailed view of the notch area to be CT-scanned.

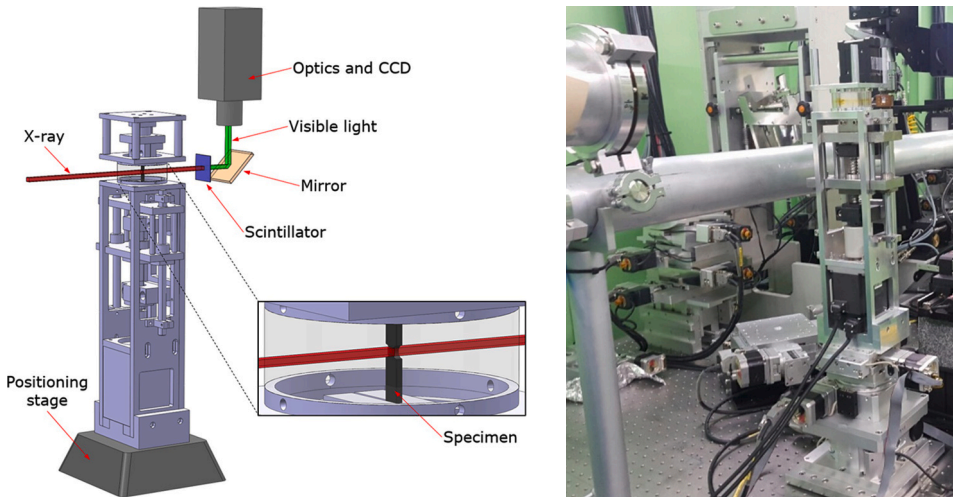

Fig. 2. (a) Schematic illustration of the *in situ* testing setup using the custom-built loading frame (b) Actual experimental setup at 6C Beamline of PAL.

radiographs is closely related to the attenuation coefficient of a constituent material. The attenuation coefficient is a function of the atomic number (Z) and photon energy (E), which is expressed as $\mu=(Z/E)^3$. This relationship implies that lower photon energy will result in higher differences in the energy absorption capability between different materials.

Fig. 3 compares mass attenuation coefficients (μ divided by density) of carbon, polymethyl methacrylate (PMMA) and iodine [18]. Carbon and PMMA are intentionally selected here since they can be considered as typical constituents of a fiber-reinforced plastic material. In Fig. 3, the difference between the attenuation coefficients of carbon and PMMA is disappearing as the X-ray energy increases. Therefore, when a sample is composed of more than two materials with similar and low densities, lower energy level should be used in order to increase greyscale contrast and distinguish the constituents in X-ray images. However, lower photon energy is not always a key solution for better image quality. When the photon energy is too low, as can be seen in Fig. 3, the attenuation coefficient is very high. This implies that the samples effectively absorb photons and leave almost nothing to be collected by a detector,

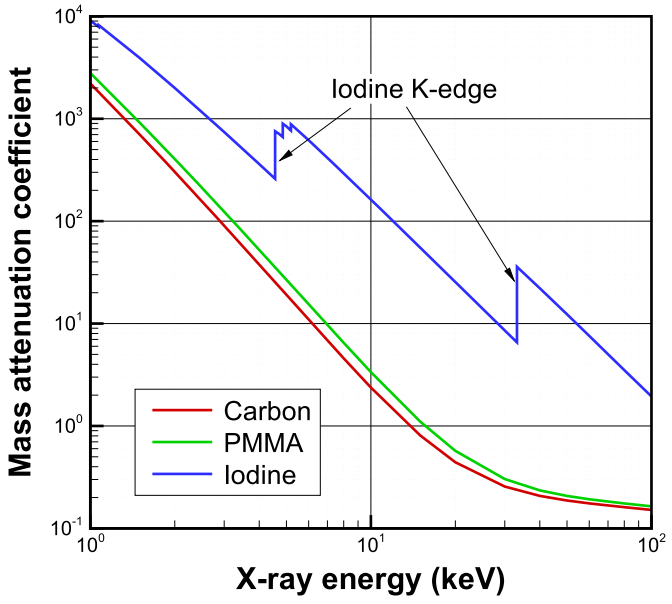

Fig. 3. Mass attenuation coefficients of carbon, PMMA, and iodine plotted on log-log axes.

leading to the darkening effect on radiographs. This can be overcome only by significantly increasing imaging time in order to receive more photons and thus acquire brighter images. In case of biomedical imaging, X-ray dose should be considered to reduce exposure time and protect patient safety as a top priority. Long imaging time is also undesirable for *in situ* testing since a specimen that is being loaded while X-ray images are taken may exhibit unexpected creep behavior or undergo additional thermal deformation due to X-rays. A sudden increase of X-ray absorption, known as K-edge [17], should also be considered regarding the energy dependency of attenuation coefficients for some materials. The low-density materials in Fig. 3 do not show significant K-edges (actually very low) whereas the K-edge of the heavy iodine is distinctly observed at around 4–6 and 30 keV.

The specimen-to-detector distance (SDD) was set to 110 mm for the present experiment. Long SDD may deteriorate the spatial resolution of X-ray images [16] and thus SDD should be short if the image resolution is a main concern. On the other hand, the edge-enhancement effect at material interfaces (see section 2.4) is linearly proportional to SDD [19]. Therefore, increasing SDD can improve the image contrast [16] with the aid of phase contrast retrieval (more information in section 2.4). The current SDD setting of 110 mm was carefully selected to enhance the contrast between fibers and a matrix material in computed tomography (CT) images with a sufficiently fine spatial resolution. The detector system consisted of a scintillator and a camera with a microscope lens. In the present test, we used a 100-μm thick $CdWO_4$ scintillator layer, a charge-coupled device (CCD) with a readout circuit for 4006 × 2672 pixels and a 10 × microscope lens. The CCD camera (PCO4000, PCO AG, Germany) has a physical pixel size of 9 μm and its maximum frame rate is 5 frames per second. The detector setup resulted in the field of view (FOV) having the size of 3.6 × 2.4 mm^2 for the projection radiography with the effective resolution of 0.9 μm/pixel. The FOV size was large enough to cover the entire volume of interest (VOI) of the specimen shown in Fig. 1(b).

If an FOV width is smaller than a sample width, beam energy absorbed by unnecessary areas of the sample outside the FOV may cause an unwanted error in reconstructed CT images. Fig. 4 illustrates a CT process of an oversized sample, which is larger than FOV width. The circular section in Fig. 4 represents the CT scanning area whose diameter is equal to the FOV width. For CT images, X-ray radiographs are first acquired at every prescribed angle of the sample. The radiographs from different angles are combined to create a three-dimensional volume (reconstruction process, see section 2.4). Fig. 4(a) and (b) depict X-ray imaging at 0 and 90-degree sample positions. When the sample is

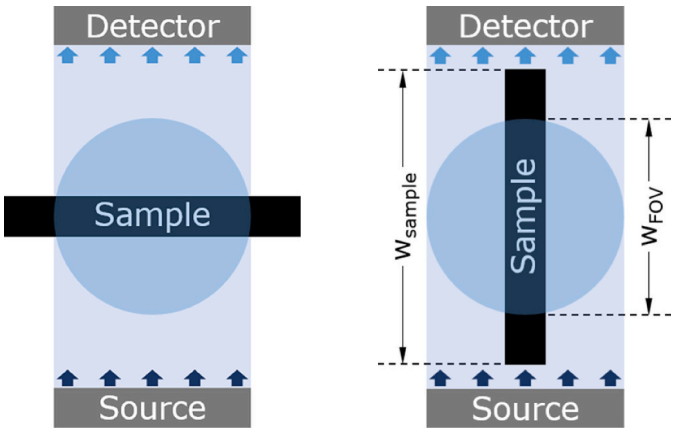

Fig. 4. Schematic illustration of CT imaging process of an oversized sample (a) X-ray imaging at 0-degree sample position (b) X-ray imaging at 90-degree sample position.

imaged at 90°, unwanted areas, initially located outside the FOV when the sample is positioned at 0°, participate to alter the X-ray beam energy to be collected by the detector. The energy absorbed in the case of Fig. 4 (b) will be lower than the correctly measured energy without the unnecessary regions. This is as if the detector records two completely different samples at 0° and 90°. Therefore, the radiographs at 0 and 90° may have a significant mismatch, resulting in erroneous CT images. In the present study, the beam size was 8 × 5 mm^2.

2.4. Tomographic reconstruction

After the X-ray projection images (radiographs) were collected, they were processed to generate multiple two-dimensional (2D) tomographic slices (tomograms) stacked vertically along the rotation axis. From the radiographs taken at different rotation angles, the linear attenuation coefficient, μ, can be calculated by the standard filtered back-projection (FBP) algorithm in each volumetric element of the object (voxel), following the Beer-Lambert law and inverse Radon transform [20]. This process of mapping μ and converting into a specific gray-scale value for each voxel is the tomogram reconstruction in the normal absorption-contrast X-ray imaging. It has been a classical method since the development of X-ray CT by Hounsfield in 1972 [21]. However, for low-density objects such as soft tissues, μ is rather low and the corresponding absorption contrast is insufficient for a clear reconstruction. As a result, the spatial resolution of CT images for such a material is usually poor. When the difference in absorption coefficients is small between two adjacent materials, the variance of their values may be partially the same, making it difficult to spatially resolve them. The two constituents of the composite specimen considered in the present study have similar atomic numbers and densities: the carbon fiber and the epoxy resin with a predominant carbon chain. Therefore, the normal absorption-contrast X-ray imaging technique is insufficient to produce distinct greyscale contrast between the two constituents. The clear intensity distribution in a CT image is a prerequisite for the successful implementation of DVC technique [14].

Synchrotron-based radiography is known to have an inherent edge-enhancement effect due to the refraction at material interfaces. The boundary of two adjacent materials is much more highlighted by the synchrotron radiation-based imaging technique than by conventional one, facilitating segmentation of different material phases [16]. The refraction can be estimated from the edge enhancement in radiographs. Known as phase retrieval, various algorithms based on certain assumptions have been developed to compute the edge enhancement [22,23]. Because the refraction effect is 100–1000 times stronger than that of energy absorption in the realm of hard X-rays, it has become a recent research focus to develop such radiographic techniques to achieve unprecedented sensitivity for imaging low density materials [16]. Therefore, this 3D image reconstruction method (named as phase-contrast reconstruction) produces a map of refractive index resulting in improved greyscale contrast.

In the present work, a stack of 2672 tomograms was obtained at each loading step with a pixel resolution of 4008 × 4008 per image, in which the physical length of one pixel is 0.9 μm. The tomograms were constructed from the radiographs using a commercial reconstruction software, Octopus (XRE, Gent, Belgium) with a filtered back-projection (FBP) algorithm combined with phase retrieval filtering, which is named as Paganin's method [23]. This method requires *a priori* knowledge about a sample and experimental condition; linear attenuation coefficient, μ and refractive index, *n* [24]. In the present study, μ and *n* of carbon at 24 keV energy level, calculated using open-source software, XOP2.4 (ESRF, Grenoble, France), were used as the input parameters for the Paganin's phase-contrast reconstruction. In general, physical properties of a dominant material can typically represent the material system.

Fig. 5 shows typical tomograms of the composite specimen reconstructed with (a) absorption-contrast and (b) phase-contrast reconstruction method, respectively. As can be seen in Fig. 5, the phase-contrast reconstruction method provides better image contrast and less noise compared with the absorption-contrast reconstruction approach. Owing to these two advantages, the phase-contrast reconstruction can more clearly capture the microstructure of a heterogeneous material, which is necessary for DVC applications. Fig. 6 depicts the VOI for DVC analysis defined on the aligned tomogram. Detailed image post-processing regarding the alignment is given in section 3.1.

3. Digital volume correlation technique

Digital volume correlation (DVC) technique has been effectively used to determine the internal volumetric deformation behavior of solid materials since it was first proposed by Bay and Smith [13,25]. After the DVC technique was first applied in the field of medical biology, various materials including soft materials [9,10], wood [11], bones [13,26], sand [27], and ceramic [28] are characterized by the 3D image analysis. An in-house DVC software has been developed [14] and utilized to study the deformation behavior inside the composite material. Since the working principle of the DVC algorithm is identical to the conventional DIC technique, the details of the in-house software is not of great concern. Instead, this section is mainly concerned with the pre- and post-processing approaches required for DVC analysis in conjunction with the *in situ* testing results.

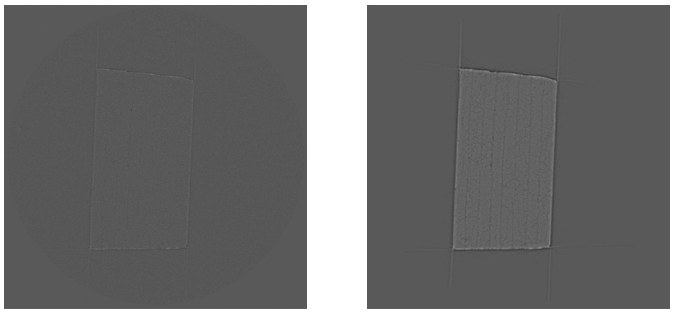

Fig. 5. Tomograms of the composite specimen reconstructed with different methods (a) Absorption-contrast reconstruction (b) Phase-contrast reconstruction (Paganin's method [23]). Note that contrast of the images are enhanced for visualization.

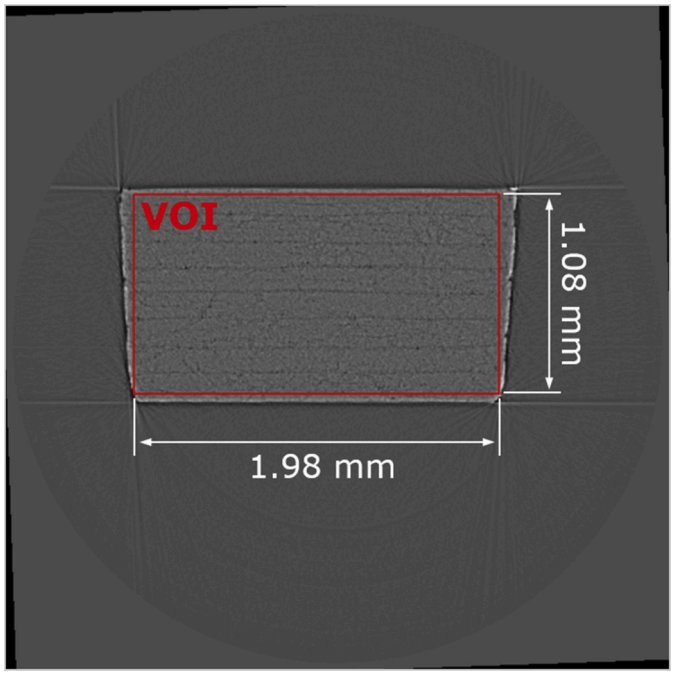

Fig. 6. Tomogram aligned for DVC analysis with the definition of a VOI region.

3.1. Correction of the initial rigid body movement of the specimen

For any mechanical loading tests, specimens at rest may undergo slight 3D rigid body rotations and/or translations as soon as a load is applied due to initial imperfections in the sample alignment, fixture installations and so on. Macroscale measurements are not greatly affected by the initial rigid body motions when the initial imperfections are insignificant. However, *in situ* testing is typically performed in the microscopic scale and thus the slight motions are not negligible even with small imperfections. If the rigid body motions are not properly corrected, the calculated deformation field may be deficient [12]. The rigid body rotation can be accounted for during the matching process between the reference and target subvolumes. Several studies [29,30] have considered an extra rotational degree of freedom (DOF) for each subvolume, especially for biomedical applications wherein a sample would undergo a large deformation. However, such an additional DOF can cause an increase in computational time during the correlation process, particularly with the increased number of subvolumes. In the present study, the composite specimen was subjected to tensile loading only. Any rigid body rotation of the subvolumes became negligible since the specimen and the components of the loading frame were firmly positioned after the tensile loading was applied. Therefore, the calibration to remove the rigid-body motions needed to be performed only once prior to the correlation process.

The initial registration of 3D CT images can be achieved using the normal vectors of the front and back surfaces of the sample as indicated in Fig. 7(a). In order to define the normal vectors, four points were picked along each of the front and back edges of a single tomogram as shown in Fig. 7(b). In doing so, the tomograms were binarized first at the inflection point in its greyscale histogram in order to distinguish the specimen from the background. As shown in Fig. 7(b), artificial lines extended from the specimen edges were also segmented by the binarization. The process of assigning points on the specimen edges was repeated on five tomograms at the interval of 0.6 mm along the *x*-direction. Total 20 points were defined on the front and back surfaces of the specimen. Then, three points were randomly selected to create a plane, except the cases in which three points were from the same tomogram, i.e., the three points were located on the same line. Total 1032 planes were defined on the front and back sides, respectively.

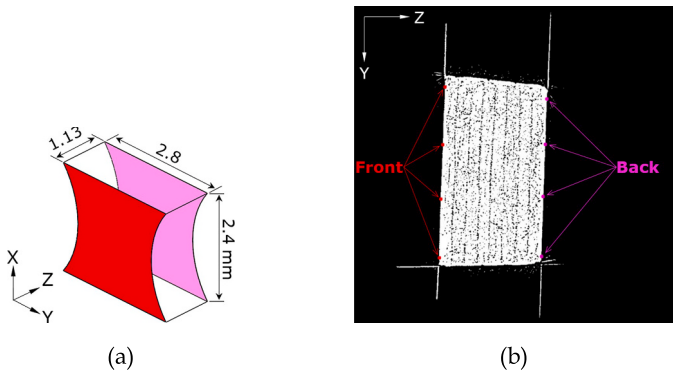

Fig. 7. Tilt correction process (a) CT scanned volume of the composite specimen (b) Four points defined on each front and back edge of the specimen.

Normal vectors were computed from all the 2064 planes and their average $\vec{n}$ was considered to represent the specimen orientation at each loading step.

As shown in Fig. 8, the normal vector, $\vec{n}_0$, corresponding to the unloaded state was compared against the normal vectors, $\vec{n}$, corresponding to the loaded states. By projecting the normal vectors to the *yz* and *xz* planes, angles between $\vec{n}_0$ and $\vec{n}$ with respect to *x* and *y* axes were obtained. The two angles are defined as θ_x and θ_y, respectively, and they are summarized in Table 1. According to the data in Table 1, the specimen was tilted a lot at the first loading step (crosshead displacement 0.02 mm) and its movement was converged near zero as the load increases. As a result, 3D CT images from each loading step were registered based on the representative normal vector of the unloaded state. The effects of the initial registration of 3D CT images will be discussed in section 4.1.

3.2. Sub-voxel registration

Since the smallest logical unit of a digital image is a pixel, the physical size of a pixel consequently determines the accuracy of displacement computed from DVC analysis. The correlation resolution is also confined by the pixel in a discrete sense. As a remedy for the limitation, sub-pixel registration algorithms have been commonly implemented in the DIC and DVC techniques [10,31–36]. It is a supplementary matching process to refine the correlation precision to achieve resolution finer than one-pixel size after integer-pixel searching. There are several sub-voxel registration methods mostly used for the DVC technique; peak-finding (PF) method [9,13], coarse-fine searching (CFS) method [31,36], Newton-Raphson iterative (NRI) method [32, 37], and gradient-based (GB) method [34,35]. The effect and necessity of implementing the sub-voxel registration algorithm into the DVC analysis has been demonstrated in Ref. [14]. In the present study, the PF method and GB method are utilized to refine the correlation precision at the sub-voxel level and their registration results were compared in section 4.2. Both methods do not consider the shape change of subvolumes, which is efficient in calculating deformations of a sample

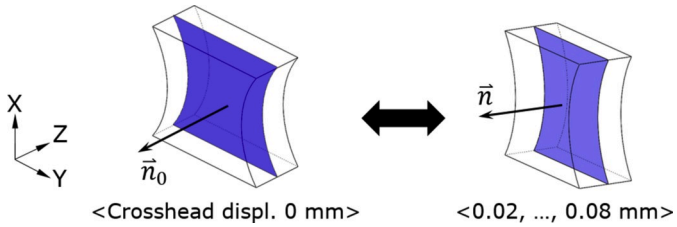

Fig. 8. Tilt correction of the specimen from 3D CT images: definition of surface normal vectors.

Table 1
Rotation angle between normal vector of 0 mm crosshead displacement step and normal vectors from other loading steps.

Crosshead displacement (mm)	θ_x (degree)	θ_y (degree)
0	0	0
0.02	0.350153	0.261064
0.04	0.399646	0.326856
0.06	0.482643	0.349826
0.08	0.52312	0.37876

subjected to a simple loading configuration.

PF method seeks a new peak position from a surface interpolating discrete correlation coefficient data. The surface typically interpolates the coefficient data of 3 × 3 × 3 or 5 × 5 × 5 voxels surrounding an initial peak position determined from an integer-voxel searching process. In the present study, a quadratic polynomial was used to create a fitting contour interpolating 3 × 3 × 3 coefficient data. From this process, new position of each subvolume at sub-voxel level can be calculated analytically by solving a system of linear equations pertaining to derivatives of the fitting function in the x, y and z directions [14]. Its robustness has been demonstrated using the *in situ* tensile test results of a polymeric material [14]. The accuracy of the fitting function may be improved by increasing the order of the polynomial function, e.g. a tricubic function. However, the analytical solution cannot be found from polynomial functions with the order of 3 or higher because the equation system composed of the derivatives of the fitting surface becomes nonlinear. A special equation solver (e.g. MATLAB `solve`) should be implemented at the cost of computation efficiency. Moreover, R-squared values for the quadratic and tricubic interpolation surfaces were both calculated to be 0.999 in average.

Gradient-based (GB) method is fundamentally based on the optical flow theory [38,39] that calculates the velocity vectors of rigid objects from time-series images. Let f and g denote the gray level values of a voxel inside the reference and target subvolumes, respectively, with the same size of $n \times n \times n$. Then, the following relation between the reference and target subvolumes holds in case of small deformations:

$$f(x_i, y_j, z_k) = g(x_i + u + \Delta x, y_j + v + \Delta y, z_k + w + \Delta z) \tag{1}$$

where i, j, k are positive integers, (x_i, y_j, z_k), are the center point coordinates of a single voxel inside the reference subvolume. u, v and w are the displacement of the target subvolume found from the integer-voxel-based DVC analysis. Δx, Δy and Δz are the additional displacement at a sub-voxel size to be determined by the GB method. The intensity function g is linearized using a Taylor series with respect to Δx, Δy and Δz

$$g(x_i + u + \Delta u, y_j + v + \Delta v, z_k + w + \Delta w) = g(x_i + u, y_j + v, z_k + w) + (g_x)_{ijk}\Delta u + (g_y)_{ijk}\Delta v + (g_z)_{ijk}\Delta w \tag{2}$$

In doing so, the 1st order derivatives of the grayscale function, g_x, g_y and g_z can be approximated by a typical numerical differentiation approach. In the present work, the central finite difference method with the 4th order accuracy is used to calculate g_x, g_y and g_z [10,34]. Combining Eq. (1) with Eq. (2) results in the following form;

$$(g_x)_{ijk}\Delta x + (g_y)_{ijk}\Delta y + (g_z)_{ijk}\Delta z = f(x_i, y_j, z_k) - g(x_i + u, y_j + v, z_k + w) \tag{3}$$

Eq. (3) can be expressed as

$$\mathbf{A}\mathbf{x} = \mathbf{b} \tag{4}$$

where

$$\mathbf{A} = \begin{bmatrix} (g_x)_{111} & (g_y)_{111} & (g_z)_{111} \\ \vdots & \vdots & \vdots \\ (g_x)_{nnn} & (g_y)_{nnn} & (g_z)_{nnn} \end{bmatrix} \tag{5}$$

$$\mathbf{x} = \{\Delta x,\ \Delta y, \Delta z\}^T \tag{6}$$

and

$$\mathbf{b} = \begin{bmatrix} f(x_1, y_1, z_1) - g(x_1 + u, y_1 + v, z_1 + w) \\ \vdots \\ f(x_n, y_n, z_n) - g(x_n + u, y_n + v, z_n + w) \end{bmatrix} \tag{7}$$

The only unknown variables Δx, Δy and Δz are determined through the least square method, resulting in a closed-form solution for $\mathbf{x}$ such that

$$\mathbf{A}^T\mathbf{A}\mathbf{x} = \mathbf{A}^T\mathbf{b} \tag{8}$$

$$\mathbf{x} = (\mathbf{A}^T\mathbf{A})^{-1}\mathbf{A}^T\mathbf{b} \tag{9}$$

4. Results and discussion

4.1. Initial registration of CT images

In this section, the effect of the initial registration described in section 3.1 is discussed by comparing the displacement results obtained with and without the correction. A partial region of the specimen is selected for the deformation analysis as indicated in Fig. 6. The cubical volume of interest (VOI), located at the center of the specimen, has the size of 2500 × 2200 × 1200 voxels or 2.25 × 1.98 × 1.08 mm^3 as shown in Fig. 9. The VOI is discretized with 6600 cubical subvolumes, where the size of one subvolume is 100 × 100 × 100 voxels. The displacement results computed along three straight lines located at $z = -0.54$ mm, $z = 0$ and $z = 0.54$ mm with $y = 0$ are compared in Fig. 10. An example of the pathline at $z = -0.54$ mm and $y = 0$ are depicted in Fig. 9. Fig. 10(a) and (b) show the displacement results along the three lines without and with the corrections, respectively. For both cases, the results are calculated using test data at 0.02 mm and 0.08 mm of the crosshead displacement. As shown in Fig. 10, the displacement results from each pathline exhibits a stepwise increasing trend with the interval of the physical size of one voxel since the sub-voxel registration (section 3.2) is not used. When the correction is not carried out, the displacement results associated with the three pathlines are different from each other as shown in Fig. 10(a) although they all exhibit increasing trends. The discrepancies imply that the specimen might be tilted during the tensile

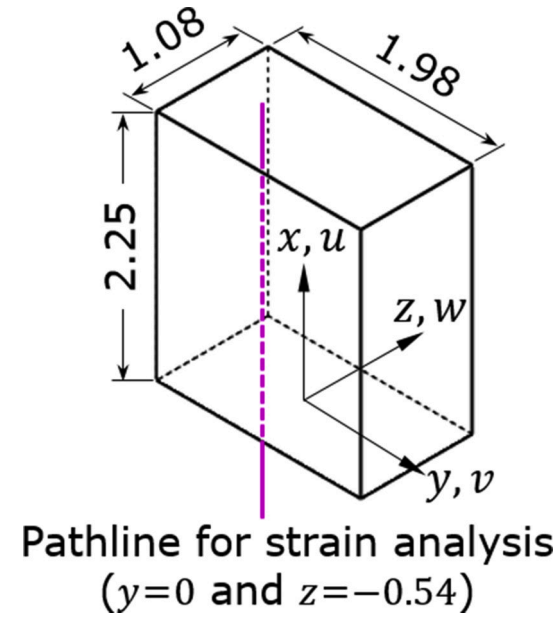

Fig. 9. Example of the definition of a pathline with the VOI dimensions (unit: millimeters).

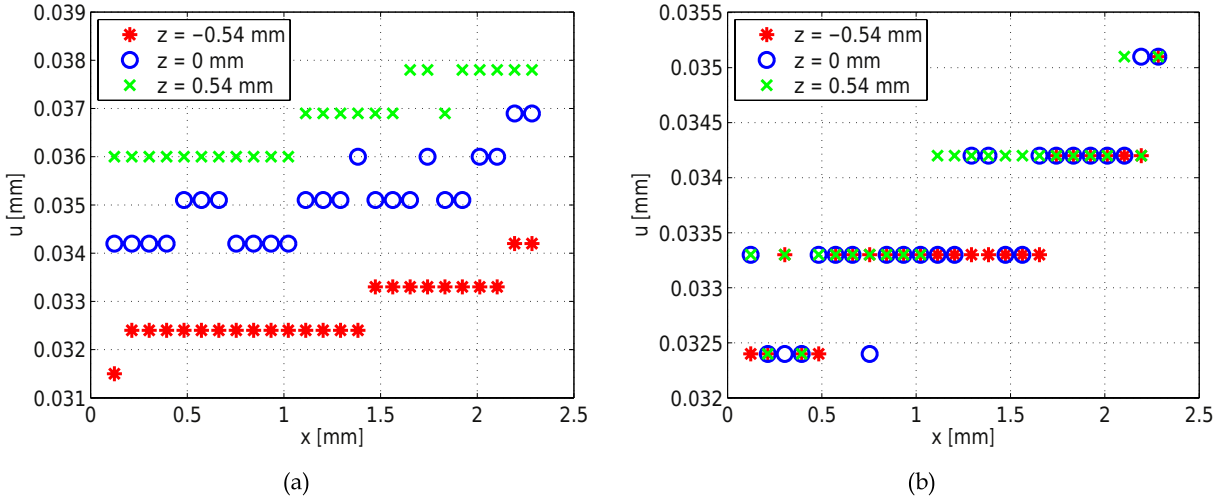

Fig. 10. (a) Displacement values computed from the DVC analysis without tilt correction (b) DVC results along the pathlines with the tilt correction approach.

test. When the tilt is corrected through the image registration approach, the results from the three pathlines are fairly consistent with each other as shown in Fig. 10(b). The comparison result emphasizes the importance of correcting a rigid body motion to accurately compute subsurface deformations using a DVC technique.

4.2. Demonstration of sub-voxel registration methods

As demonstrated in Fig. 10, DVC analysis without the sub-voxel registration results in piecewise constant displacement. Zero gradient in the displacement shall result in zero strains in the wide piecewise region. Indeed, the constant results are infeasible for a continuum material. Two sub-voxel registration methods, gradient based (GB) and peak finding (PF) methods introduced in section 3.2, are implemented into the DVC analysis and their performances are compared here. Fig. 11 (a) and (b) show the displacement values registered by GB and PF methods, respectively, along the three pathlines utilized in the prior section. Again, the deformation results are calculated using the test data between 0.02 mm and 0.08 mm. As can be seen in Fig. 11, the displacement values are now fairly continuously increasing along the loading direction for both GB and PF cases. The refined results in Fig. 11 are clearly distinguished when compared with non-registered results in Fig. 10(b).

Comparing the results exhibited in Fig. 11(a) and (b), we can observe that the displacement with the PF method shows a more monotonically increasing trend with less outliers than the results from the GB approach. The average R-square values for the three pathlines are calculated to be 0.8276 for the GB case and 0.9018 for the PF case. Both qualitative and quantitative results suggest that the PF method works better than the GB approach for the tomographic data of a carbon fiber-reinforced polymeric (CFRP) material.

Pan et al. [34]. performed DIC analysis with computer-generated speckled images and reported that the GB method shows better registration results than the PF method. Compared with the artificial image with a random speckle pattern in Fig. 12(a), a tomogram from *in situ* testing of the CFRP material in Fig. 12(b) cannot have better contrast between the pattern (fiber) and background (matrix). Such a tomogram is also vulnerable to noise and blurriness as can be seen in Fig. 11(b). The GB method should be sensitive to the contrast and noise of images since the method directly deals with intensity data of single voxels and their derivatives in a whole discrete domain (see Eqs. (1)–(9)). Whereas, the PF method is less sensitive to image quality because it utilizes correlation coefficients over a small portion near the location determined by the integer-voxel registration. Therefore, the PF method can be a better choice for the DVC analysis of inevitably noisy and blurry CT data obtained from heterogeneous materials composed of constituents with similar densities. In conclusion, DVC analysis with the sub-voxel registration can measure reasonable deformation behavior of the continuum

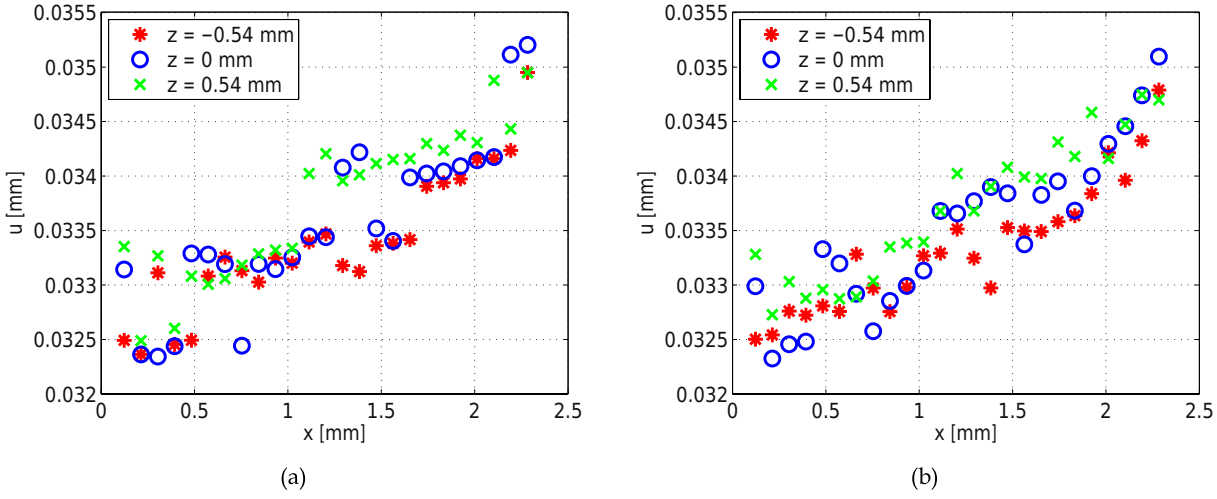

Fig. 11. DVC results along the pathlines with two sub-voxel registration methods (a) Gradient-based (GB) method (b) Peak finding (PF) method.

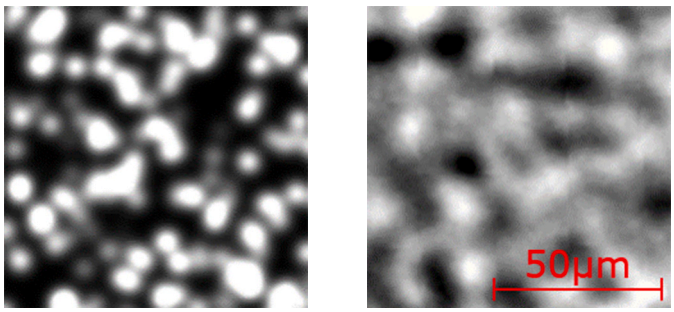

(a) (b)

Fig. 12. Contrast and noise in images (a) A computer-generated speckled image [34] (b) A tomogram of CFRP.

material.

4.3. DVC displacement results

The present DVC analysis is demonstrated with the CT data obtained from the *in situ* tensile test described in the prior section. The VOI region is selected for the deformation analysis. Displacement fields in the VOI are calculated using CT data obtained when the crosshead displacement is 0 mm and 0.08 mm. The initial image registration and the peak finding sub-voxel registration method are employed to compute the displacement. The average correlation coefficient of total 6600 subvolumes inside the VOI is 0.8739. This high correlation coefficient value indicates successful position tracking of all the subvolumes in the VOI. Note that the average correlation coefficient of the VOI region is below 0.5 with 3D CT images reconstructed without the phase retrieval filtering presented in section 2.4. The two different correlation performances highlight the importance of the reconstruction method to successfully apply the DVC technique to low-contrast tomograms. The position changes of all the subvolumes result in the displacement field of the specimen. Fig. 13(a) shows the loading-directional displacement field in the view-plane located at $z = 0.27$ mm following the coordinate system defined in Fig. 9. The displacement field is mapped on the undeformed configuration. As can be seen in Fig. 13(a), the displacement values in the field increase continuously along the loading direction.

The DVC analysis results are validated with finite element analysis (FEA) results in Fig. 13(b). Finite element (FE) model of the specimen is created with four-node shell (S4R) elements using a commercial FEA software package, ABAQUS, as shown in Fig. 14. The green region (lower grip) is fixed and the orange region (upper grip) is pulled up by 0.08 mm. The mechanical properties of the composite system have been measured and reported in Ref. [1] (see Table 2). They are used as input parameters for the FE model. For the realistic representation of the experiment, two uncertainties are considered in the FE model. First, since the center of the specimen may not be positioned at the exact center between the two grips of the loading rig, h_1 and h_2, the distances between center of the specimen and each of upper and lower grip, respectively, are different in the FE model. It is assumed that the specimen has been mounted 3 mm above the exact center, and h_1 and h_2 are set to 12 mm and 18 mm, respectively. In Fig. 13(b), FEA results of the loading directional displacement field in the VOI region (red region in Fig. 14) is plotted in the undeformed configuration. As can be seen in Fig. 13, the DVC results agree reasonably well with the FEA results; the minimum and maximum values of each contour fields are closely matching. There exists some difference between the results of DVC and FEA regarding the contour shape. This contour shape of the displacement field can be related to the fiber orientation alignment with respect to the loading direction. It is well known that the mechanical response of unidirectionally continuous fiber-reinforced composites is very sensitive to the fiber orientation. Considering the experimental setup, it is technically impossible to achieve perfect alignment while manually fastening the tiny specimen into the loading rig.

4.4. Outliers in the DVC displacement

As can be seen from the pathline analysis results in Figs. 10 and 11, there exist some outliers that are not conforming to the globally increasing trend even after the tilt correction and sub-voxel registration methods are implemented. Fig. 15(a) shows one of the extreme cases for an outlying displacement from the results obtained at the pathline of $z = 0.54$ mm. Again, the displacement results in Fig. 15 are calculated from the test data corresponding to 0 mm and 0.08 mm of the crosshead displacement. As can be seen in Fig. 15(a), the highlighted point is located far away from the band that exhibits a linearly increasing trend. Fig. 15(b) shows the displacement data without the outlier in order to visualize the increasing trend more clearly. The subvolume corresponding to the outlier in Fig. 15(a) also results in an outlying transverse displacement as shown in Fig. 15(c).

In order to investigate the source of the erroneous result, the outlying subvolume is individually examined at a single slice-image level. Fig. 16 shows the entire results of the correlation coefficients of the outlier subvolume. In principle, a typical DVC (and DIC) matching process starts by computing all the correlation coefficients while a reference subvolume is compared against each of the candidate subvolumes inside the searching area defined in the deformed state. After the maximum correlation coefficient is identified from the computation results, the reference subvolume is paired with the corresponding target subvolume and the displacement is defined from the vector connecting the center points of the two matched subvolumes. In addition to the fundamental solution, Fig. 16 compares the longitudinal and transverse distances of the 110 target subvolumes having high correlation coefficients (over 0.7). The target subvolume with the maximum C value, which is the matching result of the conventional DVC process, is marked with a green asterisk in both Fig. 16(a) and (b). As can be seen in Fig. 15(a) and (b), the loading-directional displacement, u, of the outlying subvolume (the magenta circle) should ideally be around 0.0477 mm or 53 voxels to conform to the major trend. In Fig. 16(a), four target subvolumes having the longitudinal displacement of 53 voxels are marked with blue asterisks and they are designated as Candidates (1) to (4). The same four candidates are also indicated with the same patterns in Fig. 16(b). The transverse displacement of the four candidates in Fig. 16(b) are near zero, which is an expected result. This implies that the maximum correlation coefficient may not always guarantee the correct correlation and there may exist a better candidate with a lower coefficient. The correlation coefficients (C) and displacement components of the four candidates and the C_{max} subvolume (total five target subvolumes) are summarized in Table 3.

The slice images corresponding to the five target subvolumes in Table 3 are compared with those of the reference subvolume in Fig. 17. From the cubical subvolume with the edge length of 0.09 mm as shown in Fig. 17(a), the top, middle and bottom slice-images are selected and displayed in Fig. 17(b). As can be seen in Fig. 17(b), all the middle and bottom images are similar between each other. However, the top CT images of the five target subvolumes significantly differ from that of the reference subvolume although they are similar between each other. In addition to the qualitative observations, Table 4 compares the similarities between the slice-images quantitatively through correlation coefficients computed from the conventional 2D ZNCC-based DIC technique. The quantitative comparisons also indicate the close similarities of the middle and bottom CT images, respectively, with the corresponding reference images. Despite the discrepancies of the top slices, due to the volume averaging effect in the DVC process, fairly high correlation coefficients are computed as listed in Table 3. In order to find a slice image better correlated with the top image of the reference subvolume, DIC analysis has been performed inside the 3D searching domain. As a result, several candidate facets (analogous concept of the

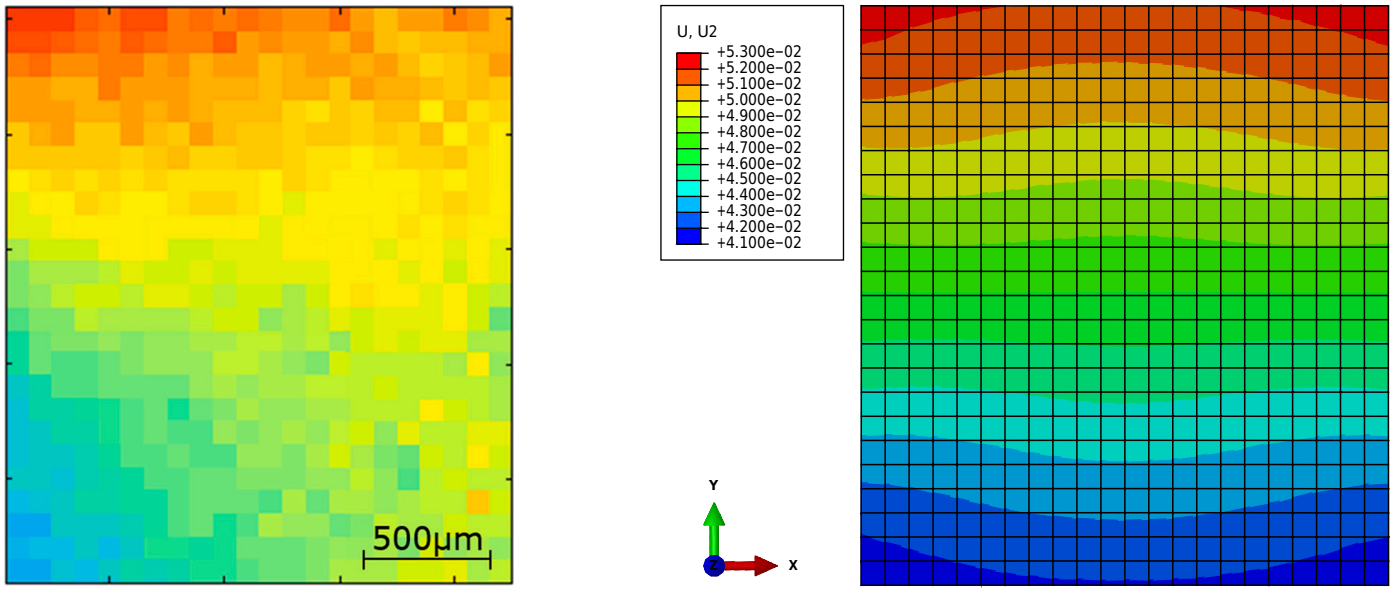

Fig. 13. Loading-directional displacement field of VOI region computed by each method (a) DVC analysis (b) Finite element analysis.

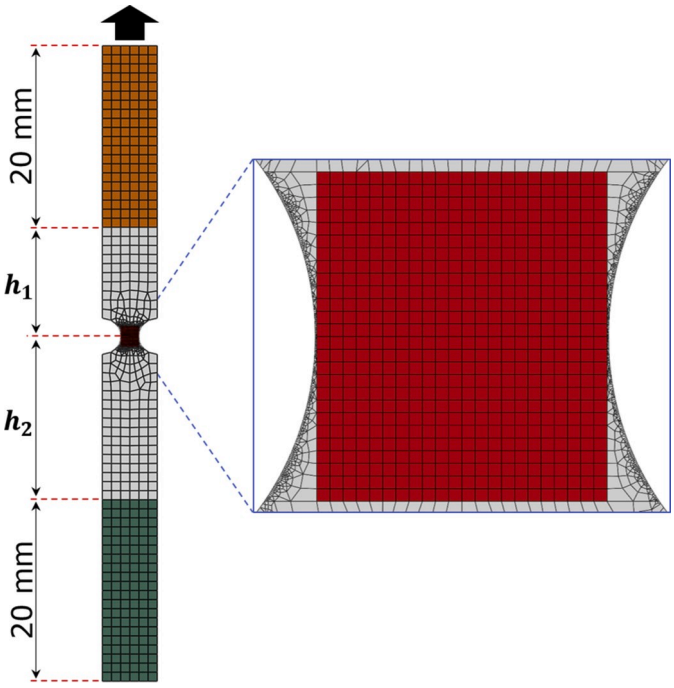

Fig. 14. Finite element model of the *in situ* testing: detailed view depicts fine structured mesh on the VOI region.

subvolume in 2D space) have been found and Fig. 18 shows one of them with the maximum correlation coefficient of 0.7622. Although the two images are quantitatively and qualitatively very similar, the target facet is located far away from the ideal position. The corresponding displacement components are $(u, v, w) = (-13,\ -1,\ 41)$ voxels, which significantly differ from the ideal values in Table 3.

Based on the results of the outlier analysis, it can be concluded that

Table 2
Mechanical properties of the UIN150/H15 composite material [1].

Properties	Values
E_{11} (GPa)	146.45
E_{22} (GPa)	7.439
G_{12} (GPa)	4.15
ν_{12}	0.338

the use of the natural pattern of a microstructure as a speckle pattern for DVC analysis might be potentially dangerous for composite materials in which similar microstructural patterns are repeatedly present in a searching domain. When we compare the displacement components of the five target subvolumes in Table 3, the four candidates are situated adjacent to each other whereas the subvolume associated with C_{max} is solely located far away from them. In spite of the physical distance, the images consisting of the C_{max} subvolume resembles those of the four candidates very closely as observed in Fig. 17(b). This outlying behavior can be explained with the microstructural pattern of the composite material considered in the present study. For the unidirectionally continuous fiber-reinforced polymer material with a high fiber volume fraction, there might exist multiple subregions having similar patterns due to the regularity of the internal microstructure. Such regions will have almost identical grayscale values on the CT images. Since the DVC process averages the intensity values of all the voxels in a subvolume, the correlation accuracy of an *individual* subvolume may be deficient.

The overall DVC results reported in Figs. 11 and 13, however, are reasonable and the correlation coefficient values are very high (more than 0.7 in general). Although there exists few similar subregions, the fiber distribution at the microscopic level is sufficiently random in a global sense to be used as a speckle pattern for the DVC analysis. The DVC technique in conjunction with *in situ* test results is still instrumental to observe subsurface deformation behavior with high resolution in a quantitative manner. The deficiency caused by the use of a natural

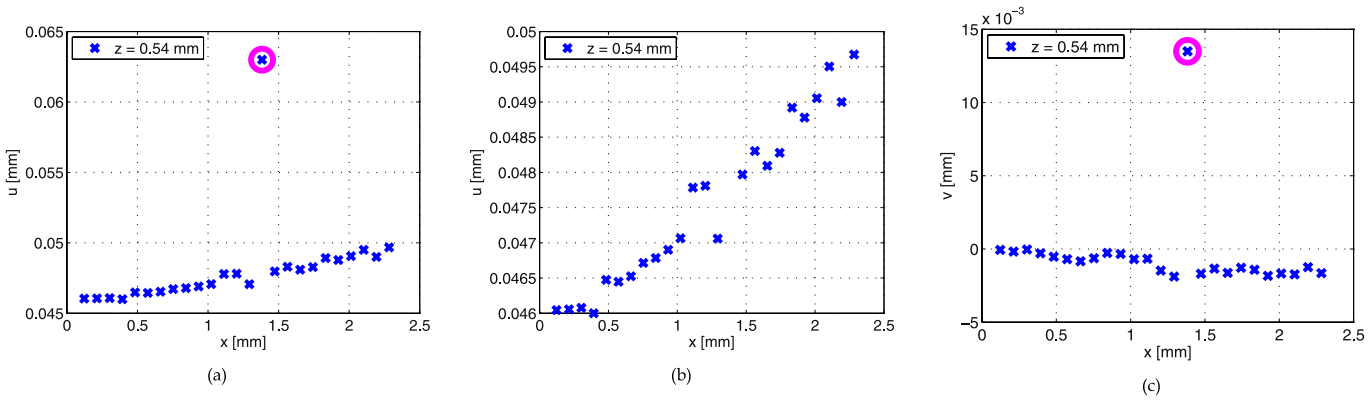

Fig. 15. DVC results along the pathline (a) An outlier in the loading directional displacement (highlighted in a magenta circle) (b) The increasing trend of the loading-directional displacement (c) The outlier in the *y*-directional displacement (highlighted in a magenta circle).

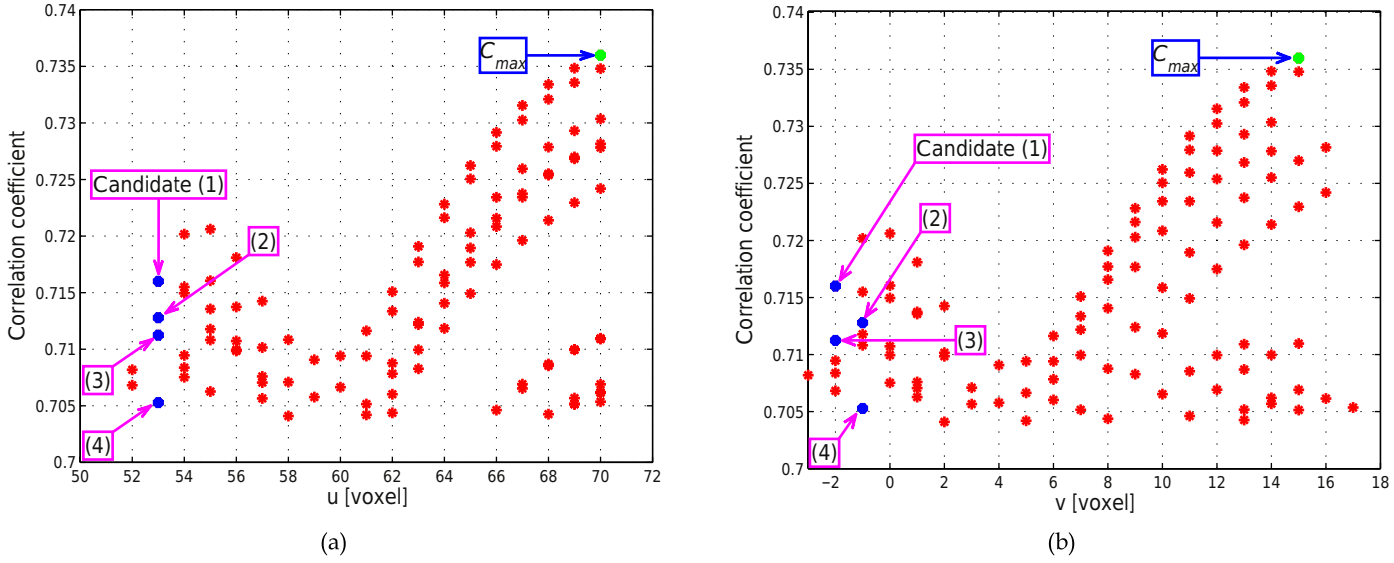

Fig. 16. Correlation results of the outlying subvolume: definition of four candidates and C_{max} subvolumes (a) C versus loading-directional displacement values of 110 target subvolumes (b) C versus *y*-directional displacement values of 110 target subvolumes.

Table 3
Correlation coefficients and displacement components of the five target subvolumes (voxel size = 0.9 μm).

Subvolume	C	u (voxel)	v (voxel)	w (voxel)
Candidate (1)	0.7160	53	−2	0
Candidate (2)	0.7128	53	−1	0
Candidate (3)	0.7112	53	−2	−1
Candidate (4)	0.7053	53	−1	−1
C_{max}	0.7360	70	15	0

Table 4
Correlation coefficients between slice-images of the reference subvolume and that of five target subvolumes.

Position of slice-images	C_{max}	Candidate (1)	Candidate (2)	Candidate (3)	Candidate (4)
Top	0.5896	0.5453	0.5524	0.5386	0.5417
Middle	0.7620	0.7756	0.7658	0.7682	0.7564
Bottom	0.7153	0.8028	0.7897	0.8108	0.7927
Average	0.6890	0.7079	0.7026	0.7059	0.6969

pattern can be remedied by implementing several state-of-the-art algorithms capable of detecting and removing an anomaly to enhance the correlation performance. When a displacement field is found for an entire domain, the volumetric data can be considered as a new image with every single voxel assigned with the corresponding displacement results instead of greyscale values. Then, image-anomaly detection techniques based on machine learning algorithms such as a support vector machine (SVM) [40] and an autoencoder [41,42] can be applied to find an outlier. After the detection process, conventional image filtering methods, e.g. median filtering, can be applied to the subregion

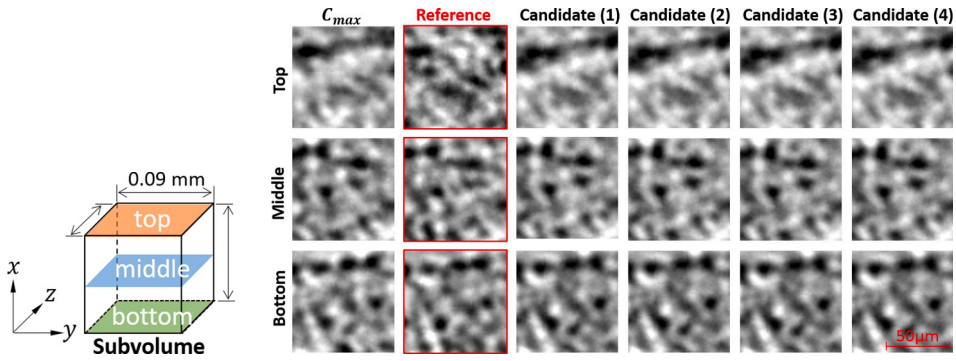

(a) (b)

Fig. 17. (a) Definition of three slice-images from a subvolume (b) Three slice-images from each reference and five target subvolumes.

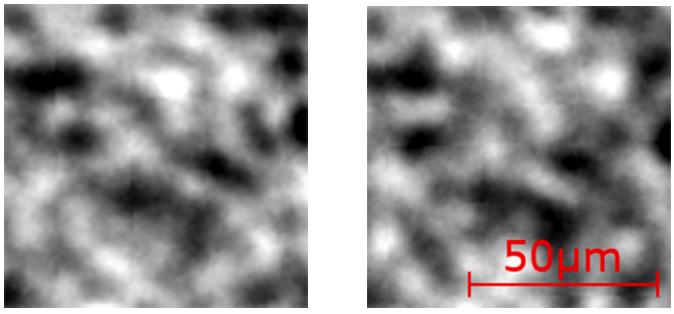

(a) (b)

Fig. 18. Correlation result of the top slice-image of outlier subvolume defined in Figs. 15 and 17(a) (a) Reference facet (top slice-image of outlier subvolume) (b) Target facet with the highest correlation coefficient.

surrounding an outlier and the outlying displacement may be replaced with a value close to ideal one.

5. Conclusion

The digital volume correlation technique has been implemented to study internal deformation behavior of a unidirectionally continuous fiber-reinforced polymer material. Main results and findings of the present work can be summarized as follows:

- DVC analysis of the composite material is performed for the first time using its natural microstructural pattern. In order to use the natural pattern, high-contrast CT images are obtained through synchrotron radiation with a phase retrieval method. The average correlation value is greater than 0.7 on a scale of 0–1, in which 1 means a perfect match.
- Methodologies to further refine the DVC results are discussed in addition to the high-contrast images. The measurement resolution is improved by implementing a sub-voxel registration method. Slight imperfections, inevitable for the small-scale *in situ* tension test, are corrected through pre-processing the CT images.
- The potential deficiency of using the natural material pattern for DVC analysis is thoroughly investigated by individually comparing raw 2D tomographic images. Although overall DVC measurements are satisfactory, few erroneous correlations can be found due to the repetition of a similar microstructural pattern.

As a concluding remark, it is reiterated that the entire pre- and post-processes of the DVC analysis are demonstrated and reported here in a great detail. The demonstration results show the successful implementation of the DVC approach to the composite material considering the high correlation coefficient values (more than 0.7). In addition to the optimal X-ray setting to distinguish the two constituents having similar densities in the CT images, it is shown that special post-image processes are inevitable to improve the accuracy of the DVC results. Initial imperfect alignment of the specimen, nontrival at the microscopic scale, is corrected by the novel image registration method. The integer-pixel resolution is overcome by implementing subvolxel registration approaches.

The limitations of the conventional correlation method based on average grayscale values are also scrutinized. While the fundamental element of an image is a pixel, the smallest units of the DVC and DIC techniques are a subvolume and a facet, respectively. They are a local group of multiple neighboring voxels or pixels. All the voxel or pixel values in the local group are first averaged in the beginning of a correlation process and the average intensity value is designated to the local group. Any conventional correlation method is basically tracking the average grayscale value in the subsequent image, not a single pixel value. In doing so, some correlation results may be erroneous if a number of groups in the images have similar average intensity values, although the overall displacement results are sufficiently accurate. In the present study, the correlation results of a single subvolume are evaluated quantitatively and qualitatively to provide a better understanding of the DVC technique using a natural pattern of the fiber-reinforced polymer material. The microstructural material pattern is analogous to a speckle pattern of a conventional DIC approach. The natural material pattern may produce a low contrast if the densities of each constituent are comparable or similar patterns are repeatedly found in a searching domain. The influence of the artificially uncontrollable natural pattern on the correlation accuracy has been thoroughly studied here. Individual slice images are compared quantitatively and qualitatively to demonstrate the results of using the material natural pattern in the DVC technique. In the present study, the poor contrast due to the similar and low densities of the carbon fiber and the epoxy material is overcome by the implementation of the phase retrieval filtering approach in the image reconstruction process.

Declaration of competing interest

The authors declare that they have no known competing financial interests or personal relationships that could have appeared to influence the work reported in this paper.

CRediT authorship contribution statement

Sooyoung Lee: Methodology, Software, Formal analysis, Visualization, Writing - original draft. **Eonyeon Jo:** Investigation. **Wooseok Ji:**

Conceptualization, Supervision, Writing - review & editing.

Acknowledgement

The authors are grateful for the support from UNIST (Ulsan National Institute of Science and Technology) through the 2020 Research Fund (1.200031.01). This work is also supported by Basic Science Research Program through the National Research Foundation of Korea (NRF) funded by the Ministry of Education (Grant No.: 2017R1D1A1B03035011). The authors are greatly indebted to Dr. Jaehong Lim at PAL for his support in the *in situ* test.

References

[1] Jo E, Lee S, Hong C, Ji W. *In situ* observation of interactive failure modes in a single-edge notched symmetric cross-ply laminate using synchrotron X-ray tomography. Compos Appl Sci Manuf 2020;128:105661.
[2] Moffat AJ, Wright P, Helfen L, Baumbach T, Johnson G, Spearing SM, Sinclair I. In situ synchrotron computed laminography of damage in carbon fibre-epoxy $[90/0]_S$ laminates. Scripta Mater 2010;62(2):97–100.
[3] Wright P, Moffat A, Sinclair I, Spearing SM. High resolution tomographic imaging and modelling of notch tip damage in a laminated composite. Compos Sci Technol 2010;70(10):1444–52.
[4] Scott AE, Mavrogordato M, Wright P, Sinclair I, Spearing SM. In situ fibre fracture measurement in carbon–epoxy laminates using high resolution computed tomography. Compos Sci Technol 2011;71(12):1471–7.
[5] Garcea SC, Mavrogordato MN, Scott AE, Sinclair I, Spearing SM. Fatigue micromechanism characterization in carbon fibre reinforced polymers using synchrotron radiation computed tomography. Compos Sci Technol 2014;99(30):23–30.
[6] Ueda M, Mimura K, Jeong TK. In situ observation of kink-band formation in a unidirectional carbon fiber reinforced plastic by X-ray computed tomography imaging. Adv Compos Mater 2016;25(1):31–43.
[7] Haboub A, Bale HA, Nasiatka JR, Cox BN, Marshall DB, Ritchie RO, MacDowell AA. Tensile testing of materials at high temperatures above 1700 C with in situ synchrotron X-ray micro-tomography. Rev Sci Instrum 2014;85(8):083702.
[8] Li Z, Guo L, Zhang L, Wang Q. In situ experimental investigation on the out-plane damage evolution of 3D woven carbon-fiber reinforced composites. Compos Sci Technol 2018;162:101–9.
[9] Franck C, Hong S, Maskarinec SA, Tirrell DA, Ravichandran G. Three-dimensional full-field measurements of large deformations in soft materials using confocal microscopy and digital volume correlation. Exp Mech 2007;47(3):427–38.
[10] Huang J, Pan X, Li S, Peng X, Xiong C, Fang J. A digital volume correlation technique for 3-D deformation measurements of soft gels. International Journal of Applied Mechanics 2011;3(2):335–54.
[11] Forsberg F, Sjödahl M, Mooser R, Hack E, Wyss P. Full Three-dimensional strain measurements on wood exposed to three-point bending: analysis by use of digital volume correlation applied to synchrotron radiation micro-computed tomography image data. Strain 2010;46(1):47–60.
[12] Mostafavi M, Collins DM, Cai B, Bradley R, Atwood RC, Reinhard C, Marrow TJ. Yield behavior beneath hardness indentations in ductile metals, measured by three-dimensional computed X-ray tomography and digital volume correlation. Acta Mater 2015;82:468–82.
[13] Bay BK, Smith TS, Fyhrie DP, Saad M. Digital volume correlation: three-dimensional strain mapping using X-ray tomography. Exp Mech 1999;39(3):217–26.
[14] Lee S, Ji W. DVC analysis of a polymer material subjected to tensile loading with synchrotron radiation tomography. Polym Test 2020;81:106204.
[15] Brault R, Germaneau A, Dupré JC, Doumalin P, Mistou S, Fazzini M. In-situ analysis of laminated composite materials by X-ray micro-computed tomography and digital volume correlation. Exp Mech 2013;53(7):1143–51.
[16] Lim J, Seo S, Kim H, Ryu CK, Rah S, Huang JY, Lee C, Seo ID, Kim S, Lee D, Cho MH. Station for structural studies on macro objects: beamline 6C bio medical imaging at the Pohang light source-II. Biodesign 2017;5(2):53–61.
[17] Bushberg JT, Seibert JA, Leidholdt Jr EM, Boone JM, Goldschmidt Jr EJ. The essential physics of medical imaging. Med Phys 2003;30(7). 1936-1936.
[18] Hubbell JH, Seltzer SM. Tables of X-ray mass attenuation coefficients and mass energy-absorption coefficients. Gaithersburg, MD, USA: National Institute of Standards and Technology; 2004 [Online] Available, version 1.4. http://physics.nist.gov/xaamdi [last accessed on March 16, 2020].
[19] Wilkins SW, Gureyev TE, Gao D, Pogany A, Stevenson AW. Phase-contrast imaging using polychromatic hard X-rays. Nature 1996;384(6607):335–8.
[20] Kak AC, Slaney M, Wang G. Principles of computerized tomographic imaging. Med Phys 2002;29(1). 107-107.
[21] Boone M, De Witte Y, Dierick M, Van den Bulcke J, Vlassenbroeck J, Van Hoorebeke L. Practical use of the modified Bronnikov algorithm in micro-CT. Nucl Instrum Methods Phys Res Sect B Beam Interact Mater Atoms 2009;267(7):1182–6.
[22] Bronnikov AV. Theory of quantitative phase-contrast computed tomography. J Opt Soc Am A 2002;19(3):472–80.
[23] Paganin D, Mayo SC, Gureyev TE, Miller PR, Wilkins SW. Simultaneous phase and amplitude extraction from a single defocused image of a homogeneous object. J Microsc 2002;206(1):33–40.
[24] Henke BL, Gullikson EM, Davis JC. X-ray interactions: photoabsorption, scattering, transmission and reflection E= 50-30,000 eV, Z= 1-92. Atomic Data Nucl Data Tables 1993;54(2):181–342 [Online] Available, http://henke.lbl.gov/optical_constants/ [last accessed on March 17, 2020].
[25] Smith TS, Bay BK, Rashid MM. Digital volume correlation including rotational degrees of freedom during minimization. Exp Mech 2002;42(3):272–8.
[26] Zauel R, Yeni YN, Bay BK, Dong XN, Fyhrie DP. Comparison of the linear finite element prediction of deformation and strain of human cancellous bone to 3D digital volume correlation measurements. J Biomech Eng 2006;128(1):1–6.
[27] Hall SA, Bornert M, Desrues J, Pannier Y, Lenoir N, Viggiani G, Bésuelle P. Discrete and continuum analysis of localised deformation in sand using X-ray CT and volumetric digital image correlation. Geotechnique 2010;60(5):315–20.
[28] Marrow J, Reinhard C, Vertyagina Y, Saucedo-Mora L, Collins D, Mostafavi M. 3D studies of damage by combined X-ray tomography and digital volume correlation. Procedia Materials Science 2014;3:1554–9.
[29] Verhulp E, van Rietbergen B, Huiskes R. A three-dimensional digital image correlation technique for strain measurements in microstructures. J Biomech 2004;37(9):1313–20.
[30] Hardisty MR, Whyne CM. Whole bone strain quantification by image registration: a validation study. J Biomech Eng 2009;131(6):064502.
[31] Sutton MA, Wolters WJ, Peters WH, Ranson WF, McNeill SR. Determination of displacements using an improved digital correlation method. Image Vis Comput 1983;1(3):133–9.
[32] Bruck HA, McNeill SR, Sutton MA, Peters WH. Digital image correlation using Newton-Raphson method of partial differential correction. Exp Mech 1989;29(3):261–7.
[33] Bar-Kochba E, Toyjanova J, Andrews E, Kim KS, Franck C. A fast iterative digital volume correlation algorithm for large deformations. Exp Mech 2015;55(1):261–74.
[34] Pan B, Xie H, Xu B, Dai F. Performance of sub-pixel registration algorithms in digital image correlation. Meas Sci Technol 2006;17(6):1615.
[35] Zhou P, Goodson KE. Subpixel displacement and deformation gradient measurement using digital image/speckle correlation. Opt Eng 2001;40(8):1613–21.
[36] Pan B, Qian K, Xie H, Asundi A. Two-dimensional digital image correlation for in-plane displacement and strain measurement: a review. Meas Sci Technol 2009;20(6):062001.
[37] Vendroux G, Knauss WG. Submicron deformation field measurements: Part 2. Improved digital image correlation. Exp Mech 1998;38(2):86–92.
[38] Davis CQ, Freeman DM. Statistics of subpixel registration algorithms based on spatiotemporal gradients or block matching. Opt Eng 1998;37(4):1290–9.
[39] Lucas BD, Kanade T. An iterative image registration technique with an application to stereo vision. In: Drinan A, editor. Proceedings of the 7th international joint conference on artificial intelligence. Vancouver: British Columbia, Canada; August . p. 674–9. Morgan Kaufmann Publishers Inc., San Francisco, CA, United States, 1981.
[40] Schölkopf B, Williamson RC, Smola AJ, Shawe-Taylor J, Platt JC. Support vector method for novelty detection. Adv Neural Inf Process Syst 2000:582–8. 2000.
[41] Hinton GE, Salakhutdinov RR. Reducing the dimensionality of data with neural networks. Science 2006;313(5786):504–7.
[42] Bhattad A, Rock J, Forsyth D. Detecting anomalous faces with 'No peeking' autoencoders. 2018. arXiv preprint arXiv,1802.05798.